IOP Conference Series: Materials Science and Engineering

PAPER • **OPEN ACCESS**

Roller profiling to increase rolling bearing performances

To cite this article: L Tudose and C Tudose 2018 *IOP Conf. Ser.: Mater. Sci. Eng.* **393** 012002

IOP Conf. Series: Materials Science and Engineering **393** (2018) 012002 doi:10.1088/1757-899X/393/1/012002

Roller profiling to increase rolling bearing performances

L Tudose[1,2] and C Tudose[2]

[1]Technical University of Cluj-Napoca, Faculty of Machine Building, Bd. Muncii 103-105, 400641 Cluj-Napoca, Romania
[2]RKB Europe, Department of Advanced Calculation and Optimization, Via Primo Agosto 1, 6828, Balerna, Switzerland

E-mail: lucian.tudose@omt.utcluj.ro

Abstract. The roller profile is of paramount importance in rolling bearing design because, under the most bearing loadings, it should provide low stresses and a long bearing life. But, unfortunately, it is impossible to find a universal optimal profile for a certain roller whatever the actual compressive load on the roller is. In the first part of this paper a complex procedure to find the optimal log-profiles of the cylindrical rollers (appropriate to specific bearing loading ranges) is presented. Since, for economic reasons, many times it is necessary to machine a simplest profile, in the second part of the paper a method to find the best 2ZB approximation (partial crowned profile) of the optimal profile of the rollers of a cylindrical roller bearing is given. The purpose is defined as an optimization problem and solved by means of Evolutionary Algorithms. To validate the optimization and considering four significant criteria, the obtained profile was compared with the optimal one and the full crowned profile used until recently.

1. Introduction

The fatigue life of any rolling bearing is strongly related to the stress state developed at the contact surface between the rollers and raceways, as well as within the material of mating parts [1-2]. Unfortunately, an analytical relationship between the geometry of the mating surfaces and the contact pressure exists only for a limited number of ideal shapes (Hertz's theory). For other shapes of the contact surfaces, a lot of efforts were done to achieve an appropriate algorithm to obtain the pressure distribution along the contact area [3-5]. In this paper, for this purpose, the conjugate gradient method (CGM) coupled with discrete convolution fast Fourier transform (DC-FFT) it was used [6-8].

Regarding the roller bearings, when a roller of finite length is pressed against a certain ring raceway (wider than the roller length) the constant pressure distribution along the roller is altered, and the end pressure tends to be significantly higher than that in the center of contact (Figure 1). This phenomenon of stress concentration is referred to as "edge loading" or "edge effect". This undesired condition is further aggravated if the rollers are misaligned for any reason: bearing mounting errors, thermal distortion of a bearing housing, elastic bending of the shaft under external loads, etc.

To counteract this condition, cylindrical rollers (and/or the raceways) should be axially "profiled", thereby making the stress distribution as uniform as possible, without edge peaks. It was Lundberg [9] who suggested for the first time such kind of profile. He found, that a profile expressed with a mathematically logarithmic curve may form, between two aligned cylinders in contact:

- an axially uniform elliptical transversely stress distribution, and
- a rectangular contact area.

IOP Conf. Series: Materials Science and Engineering **393** (2018) 012002 doi:10.1088/1757-899X/393/1/012002

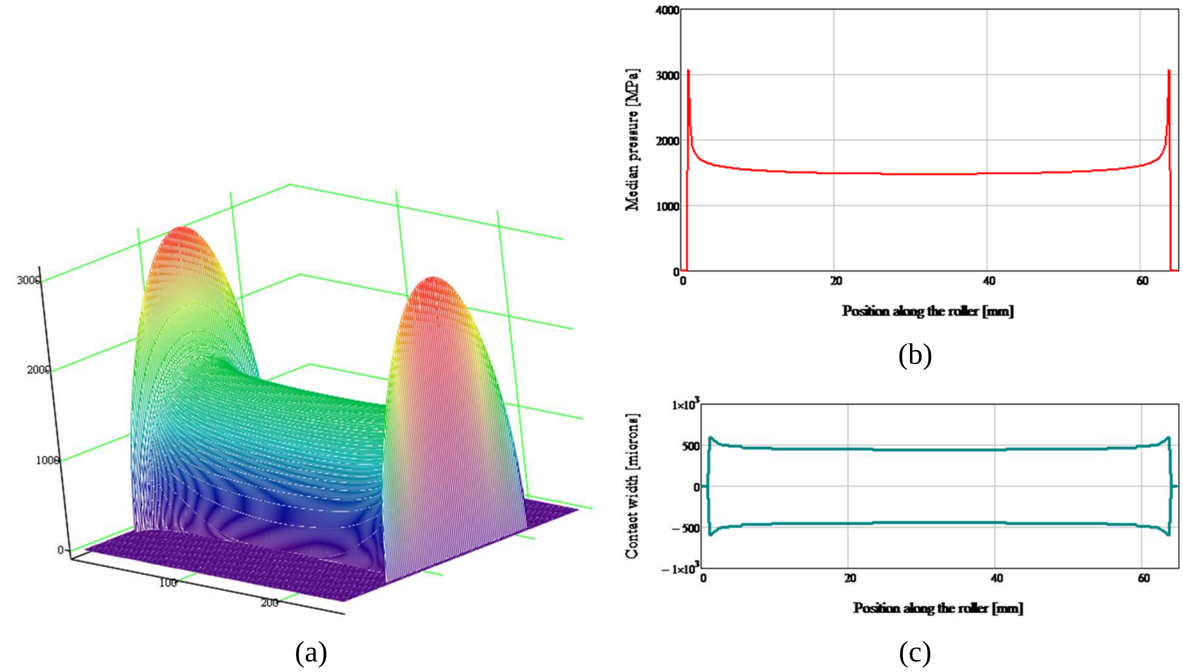

Figure 1. Pressure distribution along a roller without profile. (a) 3D distribution; (b) axial section through 3D pressure distribution; (c) “bone shape” of the contact area.

Note that ISO/TS 16281: 2008(E) [10] provides an equation of the logarithmic profile for cylindrical rollers which is essentially identical to the one proposed by Lundberg. An interesting and new proof of this equation is given in the next section.

However, Lundberg’s logarithmic profile has a major drawback: the roller radius reduction (crown drop) is theoretically infinite at the roller ends. Lundberg himself proposed an approximation to avoid this issue, but the fact that a roller has chamfers at the ends seems to solve the problem. In fact, the point where the roller profile meets the chamfer profile is a “sharp point” and, even if the resulting curve is continuous in this point, this is an important stress concentration point.

During the time, many researchers modified the Lundberg’s profile to satisfy different requirements. Johns and Gohar [11] revised the basic logarithmic function presented by Lundberg, but the crowning profile based on their equation inevitably yields edge loading when the rollers are tilted. Later, Lösche [12] brought important improvements, but his work was mostly dedicated to tapper roller logarithmic profiles and it was mention here only for historical reasons.

Fujiwara et al. [13] provided a logarithmic crowning equation by introducing three design parameters into Johns and Gohar’s formula to improve the flexibility of the profile design. That was convenient for engineering applications and offered a new design approach that prevents edge loading due to misalignment. As the authors claimed these three parameters could be optimized by applying a mathematical technique according to the operating conditions of the bearing.

On the other hand, the manufacturing of a logarithmic profile requests an expensive technology and for this reason simplified profiles were introduced. Today, there are plenty of crowning cross-section profiles including: linear profile with one crowning radius, circular crowning with large radius, ZB type roller with linear profile and two crowning radii at the end, CIR (two crowning radii) and B-TAN (three crowning radii), and so on. The authors of this paper proposed also a simplified profile, called 2ZB [14] and the subsequent improvement of this profile is given in this paper.

2. Simple proof of the profile equation given in ISO/TS 16281: 2008(E)

Consider the elastic contact of two elastic bodies presented in Figure 2. The coordinates systems $x_1y_1z_1$ and $x_2y_2z_2$ are introduced such that the axes z_1 and z_2 point into bodies *1* and *2* respectively, the axes x_1

and x_2 coincide, and the axes y_1 and y_2 (not shown in Figure 2) complete the respective right Cartesian system of coordinates. The two bodies are elastically deformed by the compressive force Q. In any cross section along the axis y_1 (or y_2), for any two points of same abscissa M_1 and M_2 one can write:

$$z_1 + z_2 + w_1 + w_2 \geq \delta \tag{1}$$

where z_1 and z_2 are the initial separation of the considered points M_1 and M_2, w_1 and w_2 are their local displacement (see Figure 2), and δ represents the displacement of a point in body 1 with respect to a point in body 2, sufficiently far from the contact zone, and situated at the same abscissa. Obviously "=" is valid if the points M_1 and M_2 are within the contact region, and ">" is in force when the mentioned points are outside of the contact region.

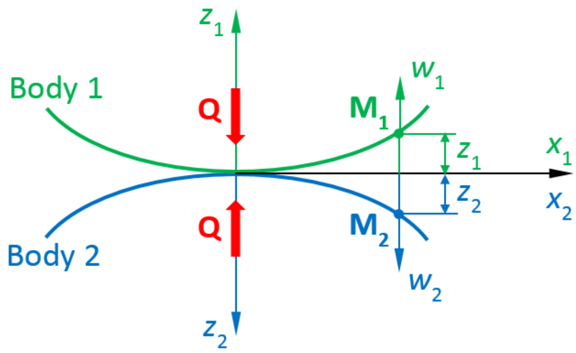

Figure 2. Two elastic arbitrarily shaped bodies in contact.

In addition to the above displacement requirements two constraints regarding the loading of the system must be considered:

1. The values of the contact pressure $P(x, y)$ between the two bodies, in any point (x, y), is positive if the point is inside the contact region, and 0 if the point is outside this region.
2. The integrated pressure distribution over the contact area D is equal to the applied load Q:

$$Q = \iint_D P(x, y)\,\mathrm{d}x\mathrm{d}y \tag{2}$$

Because the dimensions of the contact area are small with respect to the radii of curvature of the bodies in elastic contact, it has been agreed [15] that an acceptable approximation to consider that the pressure-displacement response for both bodies is identical to that of a half-space. Consequently, the following equation for the displacement at point (x, y) because of the pressure $P(x', y')$ can be used:

$$w_i(x, y) = \frac{1-\nu_i^2}{\pi E_i} \iint_D P(x', y')[(x - x')^2 + (y - y')^2]^{-1/2}\mathrm{d}x'\mathrm{d}y' \tag{3}$$

where ν_i and E_i are Poisson's ratio and the Young's modulus of elasticity for body i respectively, and D is the contact area over witch the distributed pressure acts. Combining equations (1) and (3) for any point $(x, y) \in D$ one obtains the following general equation:

$$k \iint_D \frac{P(x', y')}{[(x-x')^2+(y-y')^2]^{1/2}}\mathrm{d}x'\mathrm{d}y' + Z_1(x, y) + Z_2(x, y) - \delta = 0 \tag{4}$$

where:

$$k = \frac{1-\nu_1^2}{\pi E_1} + \frac{1-\nu_2^2}{\pi E_2} \tag{5}$$

and $Z_i(x, y)$ is the equation of the surface of body i, before the elastic deformation.

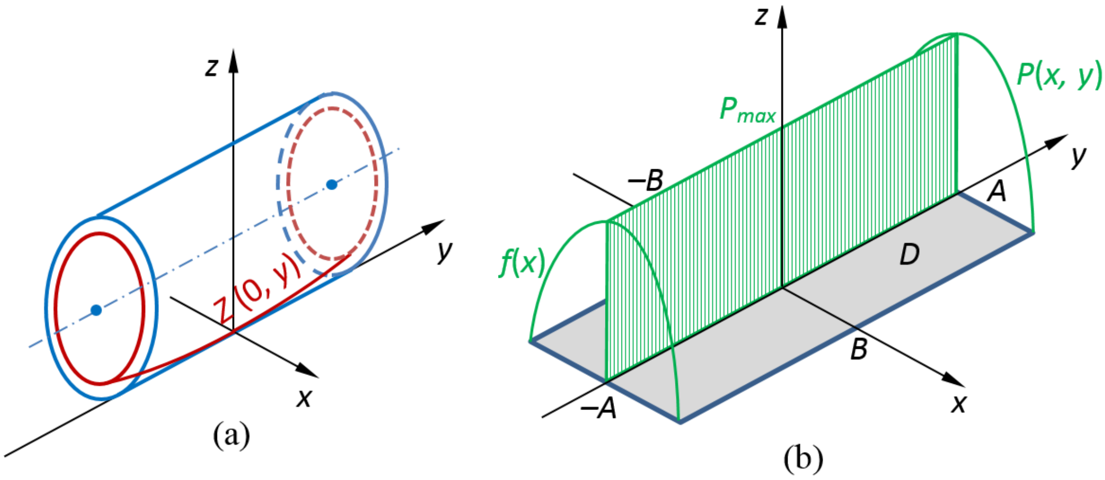

Figure 3. The elastic contact between a cylindrical roller and the plane *xy*. (a) Roller profile *Z* (0, *y*); (b) Ideal Hertzian pressure along the rectangular contact area.

The aim of this subsection is to find the equation of the cylindrical roller profile *Z* (0, *y*) such that the distribution of pressure to follow the Hertz's distribution (Figure 3) when it comes into contact with an elastic flat surface. Obviously, equation (4) becomes:

$$Z(x,y) + k\iint_D \frac{P(x',y')}{[(x-x')^2+(y-y')^2]^{1/2}}\mathrm{d}x'\mathrm{d}y' - \delta = 0;\quad (\forall)(x,y) \in D \tag{6}$$

where one wants the contact area *D* to be a rectangle

$$D = [-B,\ \ B] \times [-A,\ \ A] \tag{7}$$

and the following constraints must be considered:

$$P(x,y) = f(x);\quad (\forall)y \in [-A,\ \ A] \tag{8}$$

$$f(x) = f(-x);\quad (\forall)x \in [-B,\ \ B] \tag{9}$$

$$\max_{x\in D} f(x) = f(0) = P_{max} \tag{10}$$

$$f(B) = 0 \tag{11}$$

$$Z(0,0) = 0 \tag{12}$$

$$Z(0,y) = Z(0,-y) \tag{13}$$

Taking into account all above constraints, from equation (2) it yields:

$$Q = 4A\int_0^B f(x)\mathrm{d}x \tag{14}$$

and for *x* = 0 equation (6) becomes:

$$Z(0,y) + 2k\int_0^B f(x')\cdot g(x',y)\mathrm{d}x' - \delta = 0;\quad (\forall)y \in [0,A] \tag{15}$$

where

$$g(x',y) = \ln\frac{\left[x'^2+(y+A)^2\right]^{1/2}+y+A}{\left[x'^2+(y-A)^2\right]^{1/2}+y-A} \tag{16}$$

In the following it will be more comfortable to use *x* instead of *x*′. The composite deflection δ can now be expressed by using condition (12) in equation (15):

$$\delta = 2k\int_0^B f(x)\ln\frac{\left[\left(x^2+A^2\right)^{1/2}+A\right]^2}{x^2}\mathrm{d}x \tag{17}$$

With the above value, the following equation is obtained:

$$Z(0,y) = 2k\int_0^B f(x)\cdot G(x,y)\mathrm{d}x \tag{18}$$

where

$$G(x,y) = \ln\frac{\left[\left(x^2+A^2\right)^{1/2}+A\right]^2}{\{[x^2+(y+A)^2]^{1/2}+y+A\}\{[x^2+(y-A)^2]^{1/2}-y+A\}} \tag{19}$$

Noting:

$$x = B\cdot u \tag{20}$$

equations (14) and (18) respectively, become:

$$Q = 4AB\int_0^1 f(Bu)\mathrm{d}u \tag{21}$$

and

$$Z(0,y) = 2kB\int_0^1 f(Bu)\cdot H(u,y)\mathrm{d}u \tag{22}$$

where

$$H(u,y) = \ln\frac{\left\{\left[\left(\frac{B}{A}\right)^2u^2+1\right]^{1/2}+1\right\}^2}{\left\{\left[\left(\frac{B}{A}\right)^2u^2+\left(1+\frac{y}{A}\right)^2\right]^{1/2}+1+\frac{y}{A}\right\}\left\{\left[\left(\frac{B}{A}\right)^2u^2+\left(1-\frac{y}{A}\right)^2\right]^{1/2}+1-\frac{y}{A}\right\}} \tag{23}$$

Because

$$\left(\frac{B}{A}\right)^2u^2 = \left(\frac{B}{A}\right)^2\cdot\left(\frac{x}{A}\right)^2 \approx 0 \tag{24}$$

the following approximation is obtained:

$$H(u,y) \approx \ln\frac{4}{4\left(1+\frac{y}{A}\right)\left(1-\frac{y}{A}\right)} = -\ln\left[1-\left(\frac{y}{A}\right)^2\right] \tag{25}$$

Therefore, by using equation (21), it yields:

$$Z(0,y) \approx -k\cdot\frac{Q}{2A}\cdot\ln\left[1-\left(\frac{y}{A}\right)^2\right] \tag{26}$$

From Hertz's theory it is well known that:

$$P_{max} = \frac{1}{\pi}\cdot\sqrt{\frac{\Sigma\rho}{k}}\cdot\sqrt{\frac{Q}{2A}} \tag{27}$$

Obviously, in the case of a cylindrical roller in contact with an elastic plane:

$$\Sigma\rho = \frac{2}{D_{we}} \tag{28}$$

$$A = \frac{L_w}{2} \tag{29}$$

where D_{we} is the roller diameter and L_w is its length. If the roller and the bearing surface are made of the same material it results:

$$k = \frac{2\left(1-\nu^2\right)}{\pi E} \tag{30}$$

Eventually, substituting all above in the equation (26) one obtains:

$$Z(0,y) = -2(1-\nu^2)^2 \left(\frac{P_{max}}{E}\right)^2 D_{we} \ln\left[1-\left(\frac{2y}{L_w}\right)^2\right] \tag{31}$$

It worth noting here that if $P_{max} = 3\cdot 10^3$ MPa, E = 2.05· 10^5 MPa, ν = 0.3 the resulting equation

$$Z(0,y) = -0.00035\, D_{we} \ln\left[1-\left(\frac{2y}{L_w}\right)^2\right] \tag{32}$$

it is exactly the equation recommended by ISO/TS 16281:2008(E) [10] to be used in order to profile the cylindrical rollers of bearings.

3. Optimal profile of the cylindrical rollers of the bearings

Regarding the logarithmic profile given by equation (32) must be noted that there were several attempts to improve the carrying capacity of the contact, mainly by:

- minimization of the maximum of the contact pressure;
- maximization of rigid body displacement;
- maximization of torque or contact resultant force between the bodies;
- minimization of frictional power loss.

In this context, this research (which extends [16]) intends to draw attention to another aspect. The way in which the basic curve was obtained suggests clearly that a “logarithm” function must be involved. However, there were used a lot of simplifications and approximations, and eliminating them, probably, an analytical general equation cannot be developed. In what follows, let any roller crowning profile be called “log-profile” if it is expressed logarithmically and has the following form:

$$f(y) = drop \cdot \ln^{-1}\left[1-\left(\frac{L_w-2a_m}{L_w}\right)^{exp}\right]\cdot \ln\left[1-\left(\frac{2y}{L_w}\right)^{exp}\right]\cdot 10^{-3}\ (\mathrm{mm}) \tag{33}$$

where a_m is the distance (mm) from the lateral side of the roller where the profile *drop* (μm) will be measured, *exp* is an integer exponent lying in the range 2 … 12, and L_w is the total length (mm) of the roller. In Figure 4 all these can be followed. Note that the value of the distance a_m is set such that it exceeds the axial length of the roller chamfer. In this approach, this is considered equal to the chamfer radius.

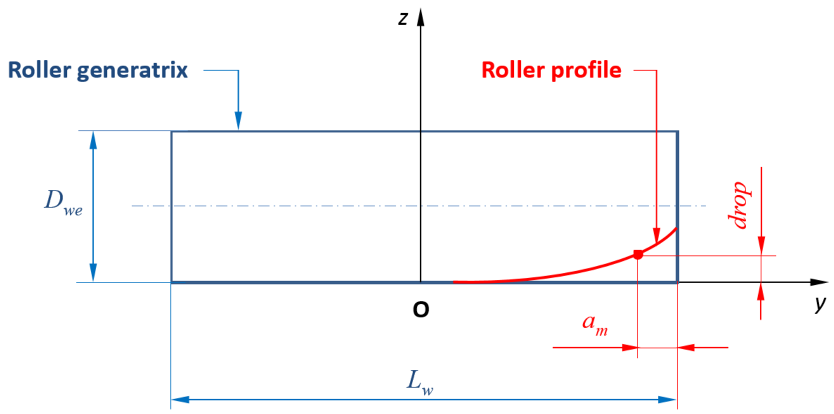

Figure 4. Design and parameters of the cylindrical roller log-profile.

In Figure 5 the same cylindrical roller, pressed against the same inner ring raceway, with the same radial load is presented. The difference consists in the axial profile: in Figure 5(a) the profile is given by equation (33), and in Figures 5(b) and 5(c) the exponent of the term ($2y/L_w$) was turned to 7 and 12, respectively (instead of 2). It is very clear that the real 3D distribution of the pressure along the contact area between the roller and raceway changes significantly, and equation (33) does not seem to be the best solution. Values of the exponent higher than 2 could provide a better (constant) distribution of the pressure. Obviously, natural questions arise: what about the constant in front of the logarithm? Can it

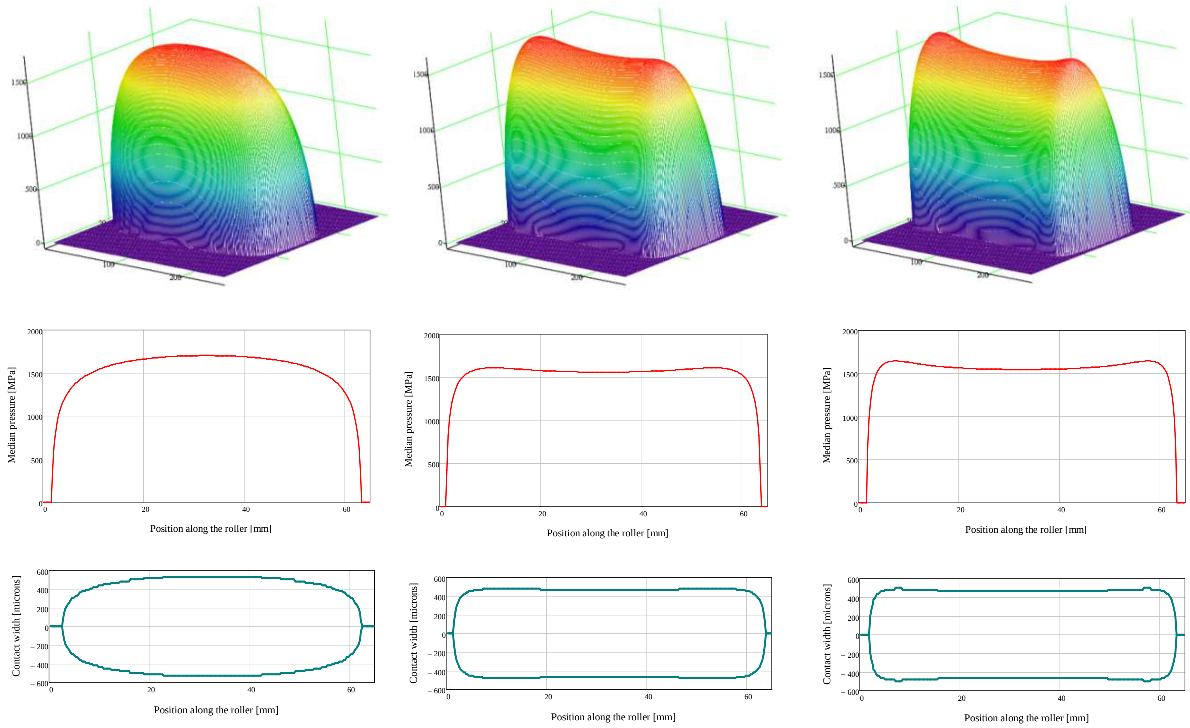

(a) (b) (c)

Figure 5. Pressure distribution for different values of *exp*. (a) *exp* = 2 (ISO); (b) *exp* = 7; (c) *exp* = 12.

modify significantly the pressure distribution? And finally: which is the best combination? The aim of this section is to answer to these questions.

3.1. Optimal profile of a given cylindrical roller

The procedure used in finding the parameters of the optimal profile equation of a certain cylindrical roller–defined by the diameter D_{we} (mm), length L_w (mm), and chamfer radius r_{ch} (mm)–is the following:

1. Consider a certain value of the maximum Hertzian pressure, P_{max} (MPa).
2. Based on ISO 15:2011 which gives the boundary dimensions of radial bearings, all possible bearings that can contains the considered rollers are identified and, for each case, the diameter of the inner ring raceway F (mm) is assumed.
   2.1. For any value of the inner ring raceway diameter F and, in addition, for $F = \infty$:
      2.1.1. Calculate, transforming the equation (28), the normal force necessary to load the roller in order to obtain, from the classical Hertz's theory, the same value of the maximum contact pressure.

$$Q = (L_{we} - 2r_h)\frac{\pi^2 k P_{max}^2}{\Sigma\rho} \tag{34}$$

where: Q is the normal force necessary that load the roller (N), r_{ch} is the roller chamfer radius (mm), k (mm^{2}N^{-1}) is a constant factor given by the equation (5) using the Young's modulus of elasticity and Poisson's ratio of the roller and inner ring material respectively, $\Sigma\rho$ is the curvature sum (mm^{-1}):

$$\Sigma\rho = \frac{2}{D_{we}} + \frac{2}{F} \tag{35}$$

2.1.2. For any assumed combination *exp* and *drop*:
   2.1.2.1. Consider the roller manufactured with the resulting profile and find the real distribution of the contact pressure between this roller and inner ring raceway using a grid (for the contact area) as large as possible.
   2.1.2.2. Store the curve given by the axial section through the obtained 3D pressure distribution.

2.2. Remove from the collected curves those that are not smooth–as in Figure 6(a)–and those that are only concave–as in Figure 6(b)–which are too close to point contact, and keep only the curves that are (from left to right, until the middle of the roller) concave and then convex–as in Figure 6(c).
2.3. Calculate the standard deviation of the values of pressures.
2.4. Order these curves, in increasing order of calculated standard deviations, and remove the worse one third of the curves.
2.5. Order the remaining curves, in increasing order of maximum contact pressure values.
2.6. Store the first five curves (five combinations of *exp* and *drop*) for each *F*.

3. Identify the most frequent combinations and accept a deal for the winning combination.

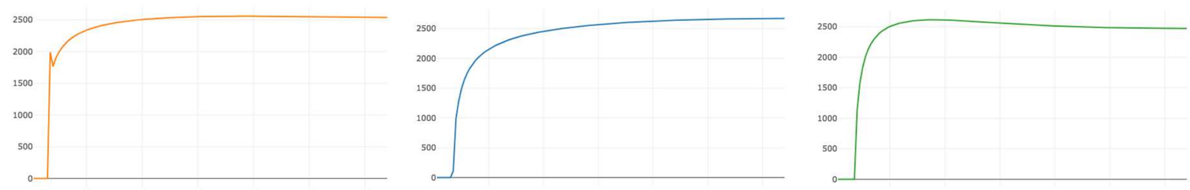

(a) (b) (c)

Figure 6. Types of pressure distributions: (a) non-smooth curve containing peaks of pressure, (b) smooth curve, but only concave and (c) concave-convex curve.

3.2. Case study

The main dimension of the considered cylindrical roller for this study are given in Table 1. For both roller and ring materials there were used E = 208 000 MPa and ν = 0.3 respectively. According to RKB Europe experience, the standard contact pressure at which the study is performed is P_{max}= 2 000 MPa. For special cases the company uses the value of P_{max}= 1 500 MPa also, as second option. In Table 2 the possible values of the diameter of the inner ring raceway are presented. The search is automatically done within the boundary dimensions provided by ISO 15:2011(E) and using the ratios given in Table 1. In Table 2 are shown also the values of the normal load necessary to obtain the assumed Hertzian pressure.

Table 1. Considered roller main dimensions and assumed ratios.

Dimension	Value (mm)	Ratio	min	max
D_{we}	32	D_{we} / [(D – d) / 2]	0.40	0.60
L_w	32	L_w / B	0.63	0.99
r_{ch}	1			

As one can observe from Table 2, a number of 17 possible bearings was identified, the appropriate F value was computed assuming that the inner and outer ring are about the same thickness, and in addition a final case was added considering the roller contact with a flat plane ($F = \infty$).

Table 2. Possible bearings and roller normal loads (to obtain a Hertzian pressure of 2 000 MPa).

No.	*F* (mm)	*d* (mm)	*D* (mm)	*B* (mm)	Thickness of the Ring (mm)	Thickness of the Rib (mm)	Dia. Series	Width Series	Dim. Series	*Q* (N)
1	108	80	200	48.0	14.00	8.0	4	0	04	41 311
2	126	100	215	47.0	12.75	7.5	3	0	03	42 705
3	133	105	225	49.0	14.00	8.5	3	0	03	43 165
4	143	110	240	50.0	16.50	9.0	3	0	03	43 759
5	163	140	250	50.0	11.50	9.0	2	1	12	44 763
6	173	130	280	48.0	21.50	8.0	3	8	83	45 192
7	188	140	300	50.0	24.00	9.0	3	8	83	45 762
8	193	160	290	48.0	16.50	8.0	2	0	02	45 935
9	263	220	370	48.0	21.50	8.0	1	0	01	47 742
10	288	240	400	50.0	24.00	9.0	1	0	01	48 196
11	348	300	460	50.0	24.00	9.0	0	0	00	49 042
12	368	320	480	50.0	24.00	9.0	0	0	00	49 267
13	488	440	600	50.0	24.00	9.0	9	0	09	50 256
14	508	460	620	50.0	24.00	9.0	9	0	09	50 378
15	673	630	780	48.0	21.50	8.0	8	0	08	49 320
16	713	670	820	48.0	21.50	8.0	8	0	08	51 120
17	758	710	870	50.0	24.00	9.0	8	0	08	51 382
18	∞	-	-	-	-	-	-	-	-	53 551

Distance from the side of the roller to the point where the profile is measured was set at a_m = 2.2 mm. The range of the search space was given by *exp* = 2 … 12 and *drop* = 2 … 12 μm. The procedure depicted in the previous sub-section was followed and the most frequent combinations were presented in Table 3.

Table 3. Simulation results.

		drop (μm) 6	8	10
exp	4			○
	5			○
	6		○	
	7		●	
	8		○	
	9	○		

The above procedure was repeated for hundreds of rollers and an interesting thing was observed: the value 7 for the exponent appears extremely often. In conclusion, to simplify the identifying process of the roller optimal profile, RKB Europe adopted an internal decision: optimal profile will always be searched for *exp* = 7. Consequently, the optimal profile of the considered roller was given by *exp* = 7 and *drop* = 8 μm. Note that for this roller ISO recommends *drop* = 15 μm (but *exp* = 2). In Figure 7 the founded optimal profile and the ISO profile for the roller in discussion are represented on the same system of coordinates. The difference is evident. Note also that 1 mm from the right side is occupied by the roller chamfer.

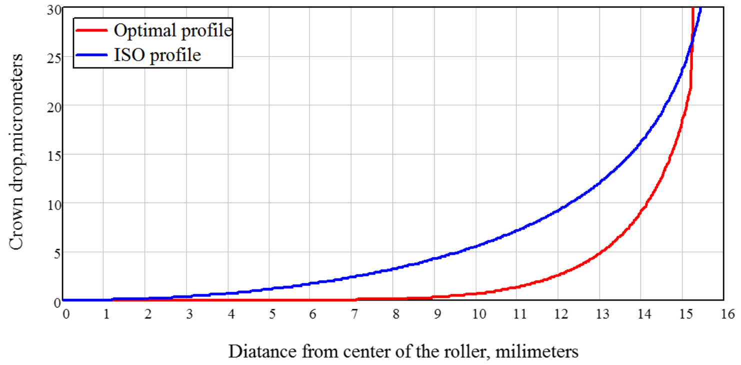

Figure 7. Optimal profile vs. ISO recommended profile.

4. Optimal approximation of the optimal profile of the cylindrical rollers

For reasons of manufacturing costs, the optimal logarithmic profile should be replaced by a simpler one, but without much loss regarding the quality of the mechanical contact. The goal of the following section is to find an optimal approximation of the optimal profile and to compare the resulted profile with the recently used profile and, eventually, with the "true" optimal profile.

4.1. 2ZB profiles

At first, RKB Europe has used the well-known "ZB profile" for its cylindrical rollers. An important step forward was made when the ZB profile was enhanced by a full crowning. This profile was used until recently and hereinafter will be called "Profile A". The proposed approximation of the optimal profile consists of a combination of two ZB profiles as presented in Figure 8 and it will be called "2ZB profile".

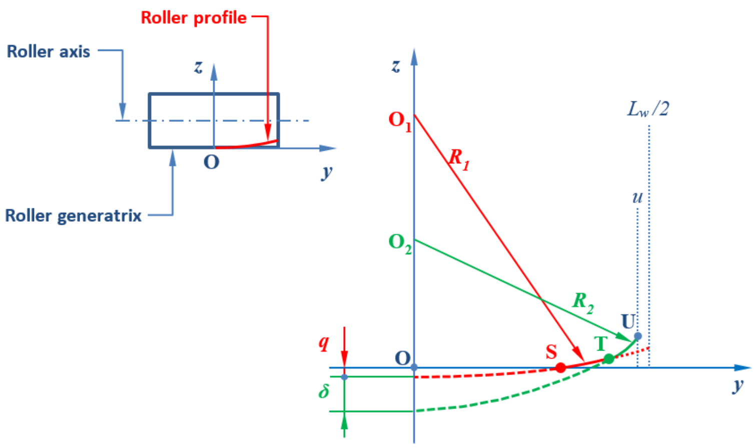

Figure 8. Definition of the 2ZB profile.

The circle of center O_1 and radius R_1 intersects the roller generatrix in S and the circle of center O_2 and radius R_2 in T. Further, the circle of center O_2 and radius R_2 intersects the chamfer profile (not represented here) in U. Consequently, the roller profile is formed by the straight-line OS, two circle segments ST and TU of radius R_1 and R_2 respectively, and, finally, by the chamfer profile. The abscissae of the points S, T, and U will be denoted by s, t, and u, respectively.

A certain 2ZB profile if fully described by only four parameters (R_1, R_2, δ, and q) and has the following equation:

$$g(y) = \begin{cases} 0, & \text{if } 0 \le y \le s \\ R_1 - q - \sqrt{R_1^2 - y^2}, & \text{if } s < y \le t \\ R_2 - (\delta + q) - \sqrt{R_2^2 - y^2}, & \text{if } t < y \le u \end{cases} \tag{36}$$

where t, s, u can be easily calculated with R_1, R_2, δ, and q.

The constraints $0 \le s < t < u < L_w/2$ (where L_w is the total length of the roller) and $R_1 > R_2$ must be satisfied. Note that if the circle of radius R_1 does not exist, the obtained profile is the old ZB cylindrical roller profile. The 2ZB profile is completely and uniquely defined by four parameters: R_1, R_2, δ, and q. Obviously, R_1, R_2, δ are strictly positive and $q \ge 0$. Even when the above mentioned constrained are satisfied there is an infinite number of combinations each representing a 2ZB profile. When $q = 0$ the circle of radius R_1 is tangent to the generatrix of the roller and a certain profile A is generated.

4.2. Multi-objective optimization

The first goal of the optimization is to find a function g whose graph is as close as possible to the graph of the optimal profile f (Figure 9). The approximation is performed along the interval $[c, u]$, where c is the greatest integer for which the condition $f(c) \le 1$ μm is still fulfilled.

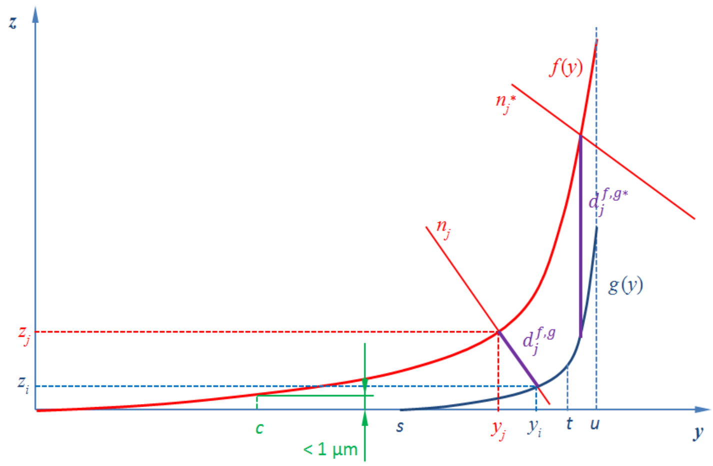

Figure 9. Approximation of the optimal profile.

It is natural to divide the interval $[c, u]$ into several subintervals of equal width and to associate to every point a corresponding distance between the graphs of the functions f and g. In this way an objective function can be easily constructed. The function f has a very special shape, especially in its last part, toward the roller side. In this part of the curve the curvature radius decreases rapidly with the increasing of y conferring a special rounding to the roller. We tried to capture this aspect by defining a special distance between the two curves, measured along the normal n_j to the graph of the function f. Obviously at the very last part of the curves (situation marked with * on Figure 9 the normal to the graph of the function f does not intersect the graph of function g in a point whose abscissa is within the interval $[c, u]$. In this case the distance will be measured vertically. For more details reader should refer to [14].

The second objective of the optimization was to "smooth" as much as possible the approximate 2ZB curve in points S and T. That means that the difference between 180° and the angle between the semi-tangents in point S (in point T as well) on the right and on the left to the graph of g must be minimized.

The obtained weighted objective function was imbedded in optimization software based initially on cuckoo search [17] and, eventually, on our cultural evolutionary algorithm [18].

4.3. Evaluation of the performances of different roller profiles

In order to evaluate the performances of different roller profiles three possible profiles of a cylindrical roller were taken into account:

1. Optimal profile (O) (considered as referential);
2. Until recently used profile A (A);
3. Optimal approximation profile (OA).

Also, as evaluation criteria, four important performance indicators were taken into account for a bearing with rollers having a certain profile and loaded with several different levels of radial load:

1. Basic rating life of the bearing (according to ISO 16281: 2008);
2. Modified rating life of the bearing (according to ISO 16281: 2008);
3. Maximum contact pressure between the most loaded roller and the inner ring raceway;
4. Maximum von Mises stress in the inner ring beneath the contact surface between the most loaded roller and the inner ring raceway and the depth at this occur.

4.4. Case study

The single-row cylindrical roller bearing NJ 320 EMP65SA (Figure 10(a)) was selected for the study of the three roller profiles behaviour under different working circumstances. The basic dynamic and static load ratings of the bearing are C_r = 389 kN and C_{0r} = 439 kN, respectively. The drawing of the rough roller is given in Figure 10(b), and the roller with classical ZB profile is shown in Figure 10(c). As one can see the roller is the same as that considered in the previous section. The radial internal clearance of the bearing is in the range RIC = 0.170 - 0.195 mm.

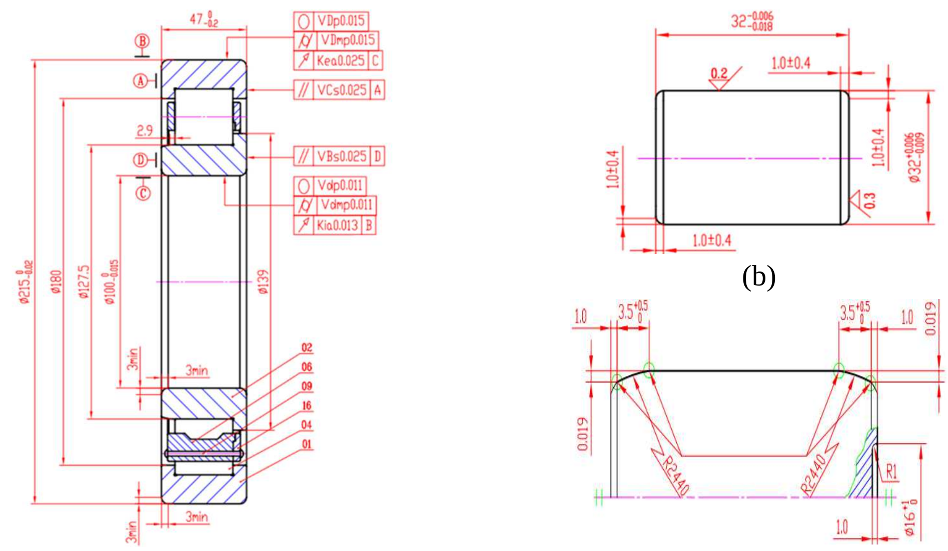

Figure 10. Case study: NJ 320 EMP65SA. (a) assembly; (b) rough roller; (c) ZB profile.

Three possible profiles of a cylindrical roller were taken into account (Table 4):

Table 4. Investigated roller profiles.

Profile	Profile type	R_1 (mm)	R_2 (mm)	δ (mm)	q (mm)	Maximum error relative to the optimal profile
O	Logarithmic	–	–	–	–	–
A	2ZB	64 000	2 440	0.027	–	4.07 μm (abscissa = 13.957 mm)
OA	2ZB	7 205	1 274	0.062	0.007	1.96 μm (abscissa = 13.853 mm)

1. Optimal profile (O) (considered as referential): a_m = 2.2 mm, exp = 7, and $drop$ = 8 μm;
2. Profile (A): full crowning of 2 μm before manufacturing the ZB profile given in Figure 10(c);
3. Optimal approximation profile (OA): obtained as it was explained in the previous sub-section.

In Figure 11 the profiles A and OA, respectively, are presented together with the optimal profile.

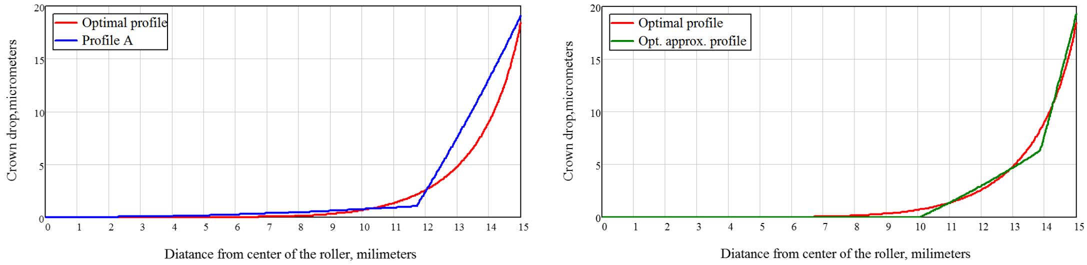

(a) (b)

Figure 11. Roller profiles. (a) optimal vs. profile A; (b) optimal vs. optimal approximation.

Three different working scenarios (loading cases) were set (as it is presented in Tables 5 and 6). Whilst speed, working temperature, lubricant, and lubrication quality were maintained the same in all three loading cases. In the first case one supposes that there is neither residual (working) radial internal clearance (RIC_w) in the bearing, nor misalignment (ψ) between the bearing bore and housing axes of symmetry, in the second case it is assumed only the presence of a certain residual internal radial clearance, and finally, in the third loading case both residual radial internal clearance and misalignment are present. Regarding the radial load level, it must be mentioned that in each case the maximum value was set very close to the value at which the most loaded roller with optimal profile O loses its performance by the occurrence of the "edge effect". Then, six levels of loads were adopted with descending step of 15 kN.

Table 5. Working conditions.

Loading case	Clearance [a] RIC_w (mm)	Misalignment [b] ψ (min)	Bearing radial load F_r (kN)	Speed n (rpm)
I	0	0	100 … 175	
II	0.100	0	85 … 160	1000
III	0.100	1.5	70 … 145	

[a] Residual (working) radial clearance.
[b] Misalignment between bearing bore and housing axes of symmetry.

Table 6. Grease lubrication conditions.

Working temp. (°C)	Cleanliness	Grease base oil	
		Kinematic viscosity at 40°C (mm^2/s)	Viscosity index VI
90	Normal	150	95

For all loading cases and for all considered loads the own software for calculating the basic rating life, modified rating life, contact pressure between all rollers and inner and outer ring raceways, von Mises stresses in rings bellow the contact surfaces was ran using a 256×128 grid for contact surface. The main results of these simulations are presented in Tables 7, 8, and 9, and in much more details, only for the loading case III, in ANNEX.

The optimal profile O demonstrated, once again, its undisputable quality and for this reason it was always chosen as referential.

4.4.1. Loading case I: $RIC_w = 0$, $\psi = 0$

In Table 7 the main results of the simulations for this case are given. Taking as referential the basic rating lives of the bearing with roller with O profile, the basic rating lives of the bearing with A and AO profiles, respectively, are given in Figure 12(a).

The basic rating lives of the bearings with OA profile are with 2- 4% lower than the referential, but they are always longer with 11.1 - 4.2% than those of the bearing having rollers with actual profile A. As one can see the difference is higher at lower loads and tends to diminish as the bearing load increases. This is easily explainable since at very high bearing loads the roller profile does not matter anymore because the huge "edge effect" cancels the beneficial presence of the profile, whatever it may be. On the other hand, as the load decreases, the difference grows significantly tending towards 15 - 20% and the advantage of the OA profile relative to the A profile becomes more evident. The behaviour of the variation of the modified bearing lives is like that of basic rating lives and for this reason is not presented here in dedicated diagrams.

Table 7. Loading case I: $RIC_w = 0$, $\psi = 0$.

Radial load (kN)	Roller profile	Rating life (hours) [a]		Max. contact pressure (MPa)	Max. von Mises stress	
		Basic L_{10h}	Modified L_{10mh}		Value (MPa)	Depth (mm)
100 = 0.26 C_r	O	6 800	12 194	1 818	1 024	0.30
	A	5 978	9 904	2 164	1 181	0.29
	OA	6 653	11 800	2 086	1 146	0.24
115 = 0.30 C_r	O	4 096	6 103	1 939	1 094	0.31
	A	3 625	5 152	2 288	1 247	0.31
	OA	3 926	5 877	2 240	1 227	0.26
130 = 0.33 C_r	O	2 539	3 552	2 052	1 158	0.34
	A	2 329	2 915	2 399	1 308	0.32
	OA	2 475	3 222	2 380	1 301	0.28
145 = 0.37 C_r	O	1 682	1 975	2 159	1 222	0.35
	A	1 563	1 757	2 681	1 554	0.07
	OA	1 639	1 898	2 510	1 371	0.29
160 = 0.41 C_r	O	1 158	1 229	2 266	1 283	0.37
	A	1 086	1 111	3 159	1 819	0.07
	OA	1 129	1 182	2 635	1 437	0.31
175 = 0.45 C_r	O	822	799	2 429	1 414	0.07
	A	774	728	3 615	2 070	0.07
	OA	802	769	2 751	1 570	0.07

[a] According to ISO/TS 16281: 2008(E).

The variation of the maximum contact pressure between the most loaded roller and the inner ring raceway versus the bearing radial load is presented in Figure 12(b). The maximum contact pressure in the case of OA profile is with 13 - 16% higher than in the similar loading condition for the O profile, but the maximum contact pressures developed in the case of the A profile represent 119 - 149% of the referential (O profile), reaching very high values for large loads. The higher the bearing radial load, the higher is the difference between the maximum contact pressures in the case A and O (or OA), respectively. Note that in absolute terms, if the bearing load exceeds 150 kN the maximum contact pressure could be far above 3000 MPa in the A profile case, whilst that in O or OA is kept at reasonable values, about 500 MPa lower.

As the bearing load increases the contact pressures between the rollers and raceways increase too and, consequently, the von Mises stresses in the rings and rollers increase as well. It is well known that a certain non-smooth profile is used, for lower loads, pecks (more or less sharp) appear in the contact pressure distribution along the contact surface between the roller and raceway. These peaks (hereinafter called *primary peaks*) are not at the edges of the contact area but somehow towards the interior. As the load increases sooner or later another edge peaks (*secondary peaks*) are developed and at a certain normal load on the roller (i.e. a certain bearing load) these peeks will become higher that the primary peaks, and the "edge effect" is fully and strongly enforced. In the studied case, the secondary pecks appear very soon (for a bearing radial load under 100 kN) in the case of A profile. There is a "delay" of about 30 MPa in the case OA and of about 60 MPa for O profile. The same differences can be observed also for the moments in which the secondary peaks exceed the primary peaks.

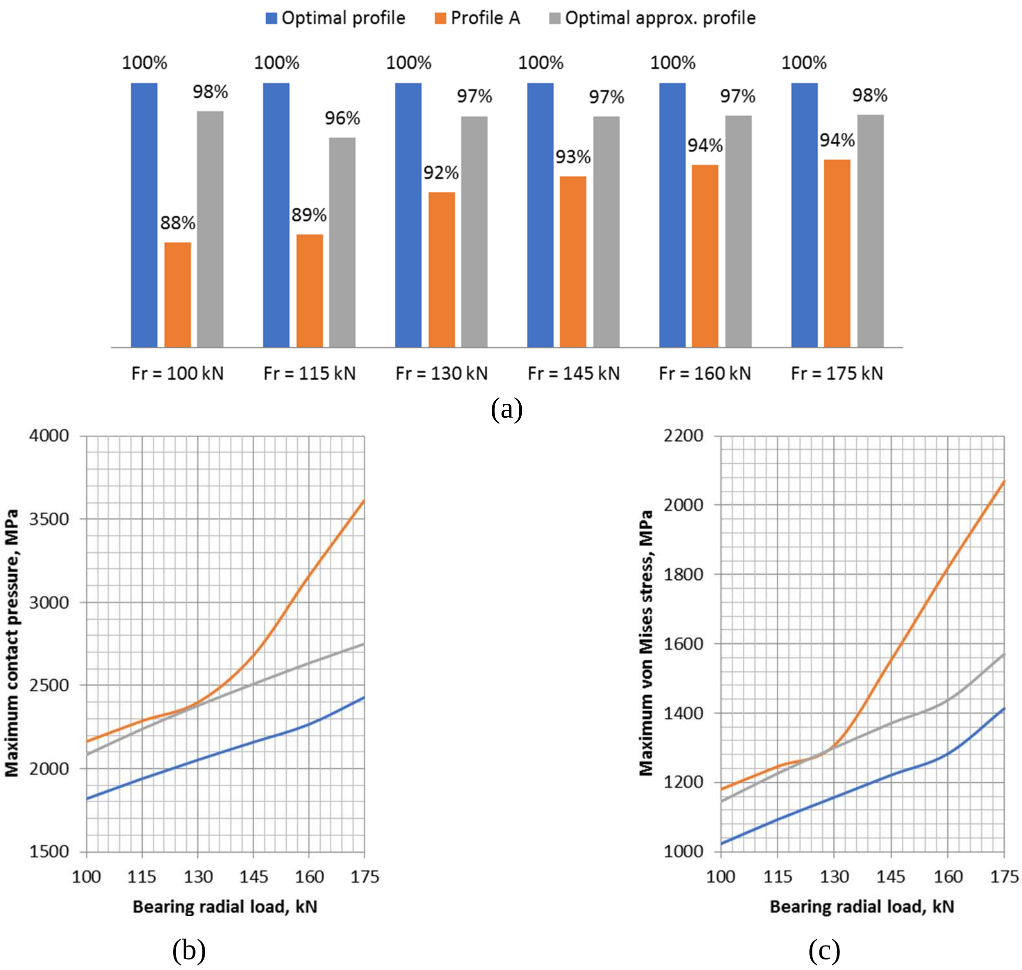

Figure 12. Loading case I: $RIC_w = 0$, $\psi = 0$. (a) Basic rating life (relative to the optimal profile O); (b) Maximum contact pressure between the roller and the inner ring raceway; (c) Maximum von Mises stress in the inner ring beneath the contact zone between the roller and raceway.

The evolution of the maximum von Mises stress in the bearing rings reflects also all these. Some deep (about 0.30 mm beneath the contact area) maxima (called hereinafter *lower maxima*) are reached and these correspond to the primary contact pressure peaks. Then, as the bearing load increases, secondary local maxima (called hereinafter *upper maxima*) appear corresponding to the secondary contact pressure peaks. Unfortunately, these upper maxima are located very close to the contact surface (about 0.07 mm!) and become very dangerous because any flaw of the material, inclusion, nano-, micro-crack, or small indentation (that easily could reach this level) will highly amplify these stresses and lead soon to the local breakdown of the ring (more likely) or roller material. Obviously, when the secondary contact stress peaks become higher than the primary peaks, the values of the upper maximum von Mises stress exceed the values of the lower maxima increasing the already mentioned risk of rings/roller material damage.

The variation of the maximum von Mises stress in the inner ring versus the bearing radial load is presented in Figure 12(c). The maximum von Mises stress in the case of OA profile is 11 - 12% higher than in the similar loading condition for the O profile, but the maximum von Mises stress developed in the case of the A profile represent 115 - 146% of the referential (O profile), reaching very high values for large loads. The higher the bearing radial load, the higher is the difference between the maximum von Mises stress in the case A and O (or OA, respectively). Note that in absolute terms, if the bearing load exceeds 150 kN the maximum von Mises stress could be far over 1700 MPa in the A profile case, whilst that in O or OA is kept bellow this value, whatever is the bearing load. It worth mentioning here that in the case of the bearing steel 100Cr6 the yield strength is of 1700 MPa, for martensitic structure and of 2000 MPa, for bainitic structure. Moreover, when the bearing load reaches 145 kN the maximum von Mises stress is located at 0.07 mm deep below the contact surface, whilst this fact happens 45 kN "later" for both O and OA profiles.

Table 8. Loading case II: RIC_w = 0.100, ψ = 0.

Radial load (kN)	Roller profile	Rating life (hours) [a]		Max. contact pressure (MPa)	Max. von Mises stress	
		Basic L_{10h}	Modified L_{10mh}		Value (MPa)	Depth (mm)
85 = 0.22 C_r	O	7 938	15 021	1 844	1 040	0.30
	A	7 065	12 380	2 197	1 196	0.28
	OA	7 766	14 525	2 120	1 164	0.24
100 = 0.26 C_r	O	4 572	7 223	1 969	1 112	0.31
	A	4 153	6 164	2 319	1 263	0.31
	OA	4 462	6 956	2 275	1 247	0.26
115 = 0.30 C_r	O	2 825	3 854	2 085	1 179	0.33
	A	2 609	3 381	2 432	1 357	0.07
	OA	2 755	3 705	2 418	1 322	0.29
130 = 0.33 C_r	O	1 842	2 222	2 195	1 242	0.36
	A	1 720	1 989	2 843	1 644	0.07
	OA	1 797	2 136	2 552	1 393	0.30
145 = 0.37 C_r	O	1 253	1 359	2 299	1 304	0.37
	A	1 177	1 233	3 326	1 911	0.07
	OA	1 222	1 308	2 676	1 459	0.32
160 = 0.41 C_r	O	881	872	2 604	1 509	0.08
	A	830	795	3 781	2 161	0.07
	OA	860	840	2 891	1 666	0.07

[a] According to ISO/TS 16281: 2008(E).

4.4.2. Loading case II: RIC_w = 0.100 mm, ψ = 0

The results of the simulations corresponding to this loading case are presented in Table 8. Taking as referential the basic rating lives of the bearing with roller with O profile, the basic rating lives of the bearing with A and AO profiles, respectively, are given in Figure 13(a).

The presence of the bearing radial internal clearance leads to a decreasing of the bearing lives in all cases and for all profiles by about 28% relative to the values obtained in the simulations corresponding to the first loading case. The basic rating lives of the bearings with OA profile are about 2% lower than in the case O, but they are longer with 10.1 - 4.2% than those of the bearing having rollers with profile A and the difference is higher at lower loads and tends to diminish as the bearing load increases. As the load decreases, the difference grows significantly and clearly tends towards higher values as 15 - 20%.

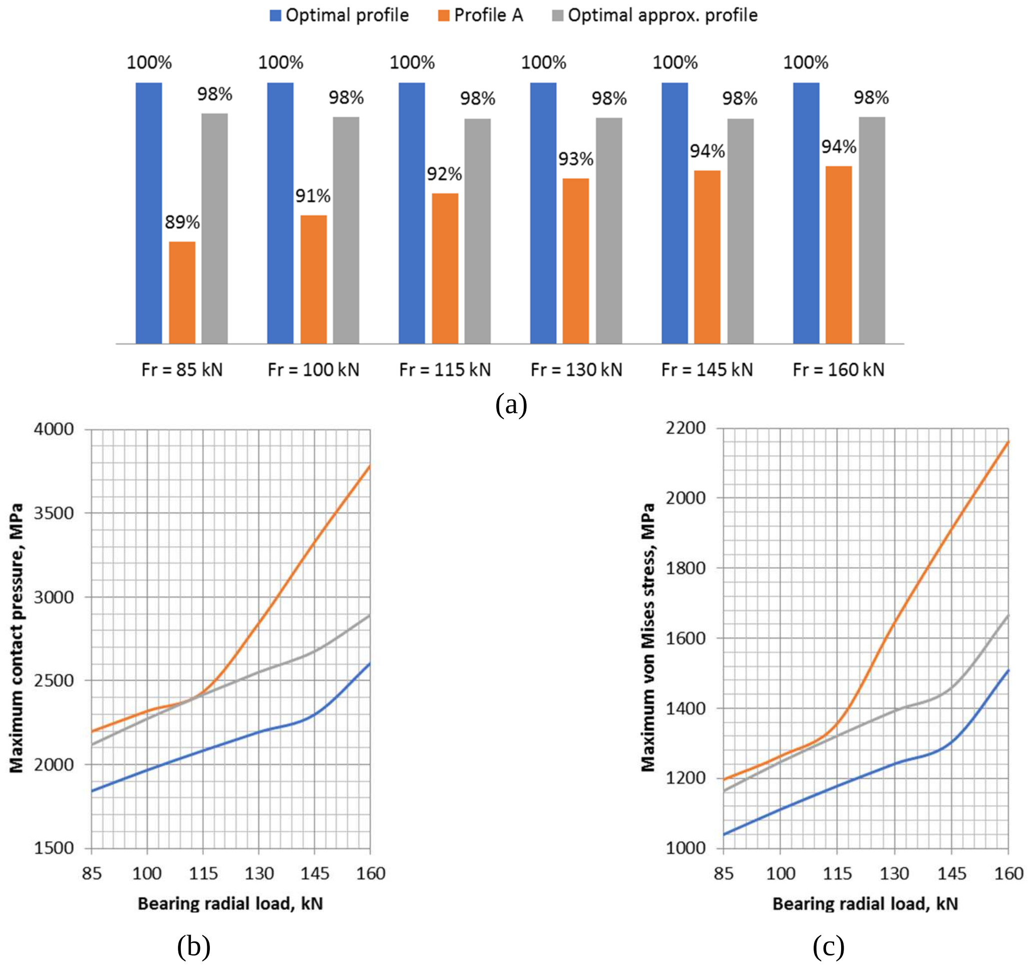

Figure 13. Loading case II: $RIC_w = 0.100$, $\psi = 0$. (a) Basic rating life (relative to the optimal profile); (b) Maximum contact pressure between the roller and the inner ring raceway; (c) Maximum von Mises stress in the inner ring beneath the contact zone between the roller and raceway.

The variation of the maximum contact pressure between the most loaded roller and the inner ring raceway as function of the bearing radial load is presented Figure 13(b). The maximum contact pressure in the case of OA profile is 11 - 15% higher than those in the case of the O profile, but the maximum contact pressures in the case of the A profile represent 119 - 145% of the referential (O profile). The higher the bearing radial load, the higher is the difference between the maximum contact pressures in the case A and O (or OA), respectively. If the bearing load exceeds 130 kN the maximum pressure could be far above 3000 MPa in the A profile case, whilst that in O or OA is kept at much lower values.

The secondary pecks appear very soon (for a bearing radial load under 85 kN, lower that in the previous loading case) in the case of A profile, after a “delay” of about 30 MPa in the case OA and of about 60 MPa for O profile. The same differences can be observed also for the moments in which the secondary peaks exceed the primary peaks.

The variation of the maximum von Mises stress in inner ring versus the bearing radial load is presented in Figure 13(c). The maximum von Mises stress in the case of OA profile is with 10 - 12% higher than in the similar loading condition for the O profile, but the maximum contact pressures in the case of the A profile are with 15-47% higher than those developed in the case of the referential (O profile), reaching very high values for large loads. The higher the bearing radial load, the higher is the difference between the maximum von Mises stress in the case A and O (or OA), respectively. If the bearing load exceeds 135 kN the maximum von Mises stress could be far above 1700 MPa in the A profile case, whilst that in O or OA is kept more or less bellow this value, whatever is the bearing load. Moreover, when the bearing load reaches about 115 kN the maximum von Mises stress is at 0.07 mm deep bellow the contact surface, whilst the lower maxima of the maximum von Mises stress become preponderant about 45 MPa "later" (for both optimal O and optimal approximation OA profiles).

4.4.3. Loading case III: RIC_w = 0.100 mm, ψ = 1' 30"

In table 9 the results of the simulations corresponding to the third loading case are given. The basic rating lives of the bearing with profiles O, A and AO, respectively, are given in Figure 14(a).

Table 9. Loading case III: RIC_w = 0.100, ψ = 1' 30".

Radial load (kN)	Roller profile	Rating life (hours) [a]		Max. contact pressure (MPa)	Max. von Mises stress	
		Basic L_{10h}	Modified L_{10mh}		Value (MPa)	Depth (mm)
70 = 0.18 C_r	O	12 713	26 332	1 895	1 073	0.30
	A	11 448	21 886	2 257	1 226	0.30
	OA	12 356	24 927	2 257	1 229	0.25
85 = 0.22 C_r	O	6 871	11 707	2 026	1 149	0.33
	A	6 274	10 042	2 383	1 346	0.07
	OA	6 677	11 102	2 407	1 308	0.28
100 = 0.26 C_r	O	4 049	5 891	2 150	1 221	0.35
	A	3 738	5 172	2 859	1 652	0.07
	OA	3 937	5 602	2 552	1 384	0.30
115 = 0.30 C_r	O	2 544	3 245	2 264	1 288	0.36
	A	2 365	2 891	3 367	1 932	0.07
	OA	2 473	3 091	2 685	1 454	0.32
130 = 0.33 C_r	O	1 678	1 913	2 639	1 523	0.09
	A	1 566	1 715	3 842	2 193	0.07
	OA	1 633	1 828	2 945	1 695	0.07
145 = 0.37 C_r	O	1 151	1 191	3 104	1 776	0.08
	A	1 074	1 076	4 295	2 441	0.07
	OA	1 120	1 138	3 406	1 948	0.07

[a] According to ISO/TS 16281: 2008(E).

The presence of the bearing residual radial internal clearance and misalignment between the bearing bore and housing axes leads to a decreasing of the bearing lives in all cases and for all profiles by about 35% relative to the values obtained in the simulations corresponding to the first loading case, that means about 7% decrease due to the misalignment. The basic rating lives of the bearings with OA profile are about 3% lower than in the case O, but they are longer with 7.7 - 4.3% than those of the bearing having rollers with actual profile A. As in the previous cases the difference is higher at lower loads and tends to diminish as the bearing load increases. As the load decreases, the difference grows towards 15%.

In Figure 14(b) is shown the variation of the maximum contact pressure (in absolute values) between the most loaded roller and the inner ring raceway as function of the bearing radial load. The maximum contact pressure in the case of OA profile is with 10 - 19% higher than those in the case of the O profile, but the maximum contact pressures in the case of the A profile represent 119 - 138% of the referential (O profile). The higher the bearing radial load, the higher is the difference between the maximum contact pressures in the cases A and O (or OA), respectively. If the bearing load exceeds 100 kN the maximum contact pressure could be far above 3000 MPa in the A profile case, whilst that in O or OA reaches significantly lower values. Moreover, in the case of the actual profile A, for bearing loads over 140 kN is very likely that the deformations of the mating parts (roller and inner ring) to enter in the zone of plastic deformations.

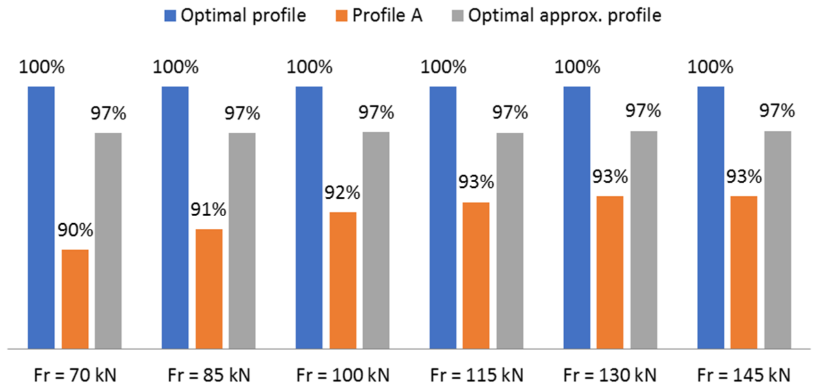

(a)

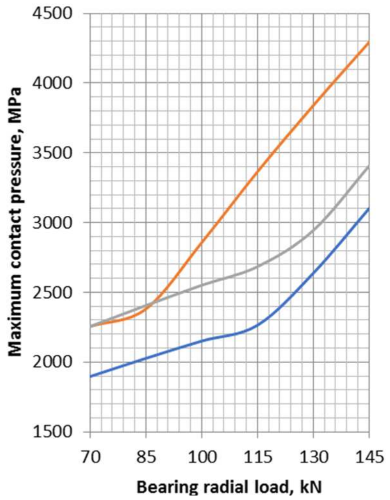

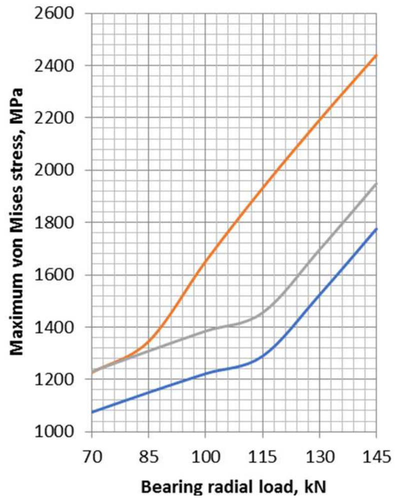

(b) (c)

Figure 14. Loading case III: RIC_w = 0.100, ψ = 1' 30". (a) Basic rating life (relative to the optimal profile); (b) Maximum contact pressure between the roller and the inner ring raceway; (c) Maximum von Mises stress in the inner ring beneath the contact zone between the roller and raceway.

As one can see from Table A1 or Table A2 from ANNEX, in the case of A profile, the secondary pecks appear very soon, for a bearing radial load about 60 kN (lower that in the previous loading case). That means about 15% of bearing dynamic load rating (that is a very common loading case in real world applications). It must be mentioned that the appearance of the first secondary pressure peaks is, again, after a “delay” of about 30 MPa in the case OA and of about 60 MPa for O profile. The same differences can be observed also for the moments in which the secondary peaks exceed the primary peaks.

The variation of the maximum von Mises stress in inner ring versus the bearing radial load is given in Figure 14(c). The maximum von Mises stress in the case of OA profile is with 10 - 15% higher than in the similar loading condition for the O profile, but the maximum contact pressures in the case of the A profile are with 14 - 37% higher than those appeared in the case of the optimal O profile, reaching, as expected, very high values for large loads. The higher the bearing radial load, the higher is the difference between the maximum von Mises stress in the case A and O (or OA), respectively. If the bearing load exceeds 100 kN the maximum von Mises stress could be far above 1700 MPa in the A profile case, whilst that in O or OA is kept bellow this value, whatever is the bearing load. Moreover, when the bearing load reaches about 85 kN the maximum von Mises stress is located at 0.07 mm deep below the contact surface, whilst the lower maxima of the maximum von Mises stress become major about 45 MPa “later” (for both optimal O and optimal approximation OA profiles).

5. Conclusions

Examining the simulation results in all three assumed loading cases some important remarks and conclusions can be drawn:

1. The optimal profile O is indeed the best from all points of view assumed in this research;
2. Whatever is the criterion the optimal approximation profile OA follows constantly the behavior of the optimal profile O (the curves of any considered parameter for OA and O profile are somehow “parallel”);
3. The above statement is not valid for the actual profile A, when large or even very large variations (relative la O profile behavior) can be observed;
4. Comparing the behavior of the profiles A and OA one can concluded that in any working circumstances and in any loading conditions the OA profile is better than the actual A profile with the following remarks:
   a) At lower loads bearing with OA rollers exhibit an increased life with up to 20% than the bearing with A rollers. On the other hand, for both profiles, the maximum contact pressure and the maximum von Mises stress are in the same range;
   b) At high loads bearing life is somehow independent of the profile used for the rollers, but the values of the maximum contact pressure and the maximum von Mises stress in the case of OA profile are up to 35% lower than the similar values obtained for the actual A profile. Note that this happens even in the case when the bearing works at low loads, but sometimes overloads and shocks appear.

In the case of the A profile the influence of residual internal clearance and misalignment is stronger than in the case of OA profile. For example, taking as referential what happens in conditions of zero clearance and misalignment, in the case of A profile, for loads over 90 kN the maximum contact pressure increases with 50 - 60%, when the clearance and misalignment are present. For the OA profile the increase is only about 25 - 35%.

The same behaviour can be observed when one considers the criterium of the maximum von Mises stresses in the inner ring material beneath the contact between the roller and ring raceway. Moreover, the presence of the maximum von Misses stress at very lower depth occurs at lower bearing radial loads in the case of A profile with respect to profiles O or OA.

In addition is worth noting here that under the same light load, a fully crowned roller does not use the total length of the roller, and for these reason, the partially crowned roller experiences less contact stress. Under the same heavier load for a crowned profile the contact stress in the center of the contact can greatly exceed that in a partially crowned or even straight profile contact. That is the reason for what we believe (as many others, see for example [1] and [19]) that it is preferable the 2ZB profile instead of a full crowned one.

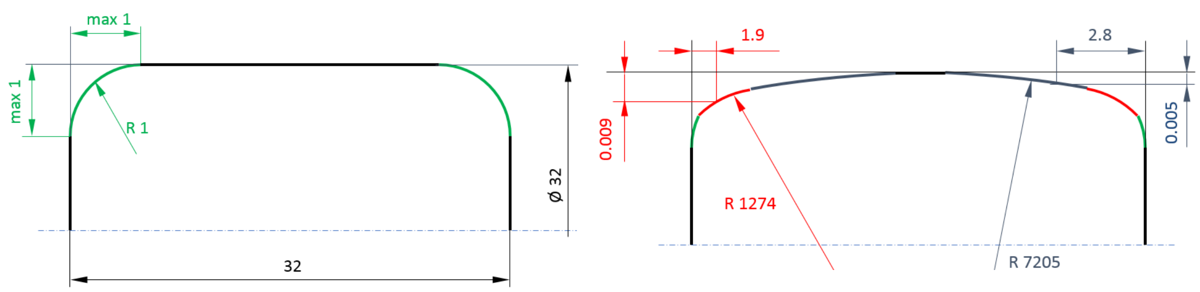

Figure 15. Drawing of the roller with the obtained OA profile.

All these make the OA profile very competitive, and with the observation that from technological point of view there is no difference between the OA and A profiles, in Figure 15 is given the drawing of the roller with OA profile.

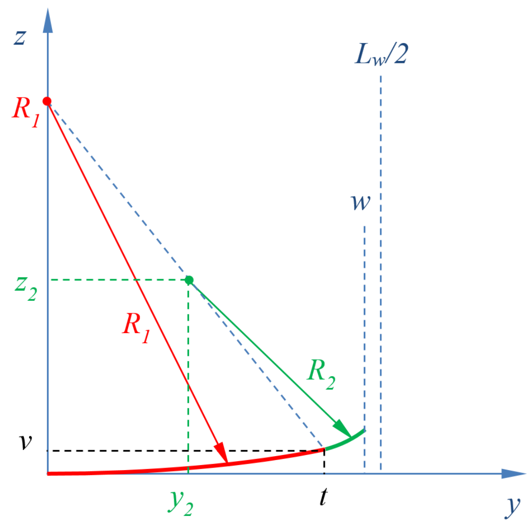

Figure 16. Smooth partially crowned profile (S2ZB).

Once the necessary technology will become enough cheap, the next approach will be the use of the smooth 2ZB profile (S2ZB), presented in Figure 16, in the approximation of the optimal log-profile. In this way one pressure peak will be removed with significantly positive results.

Acknowledgments
The authors would like to thank the RKB Group, the Swiss bearing manufacturer, for the permission to publish these results and the RKB staff for their great interest and support during the development of this project.

Appendices
Tables A1-A4.

Table A1. Loading case III. Axial section through the contact pressure distribution.

F_r	Optimal profile	Profile A	Optimal approx. profile
70 kN	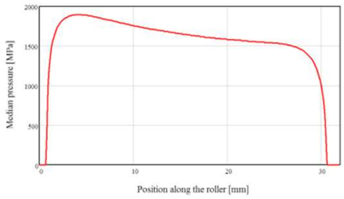	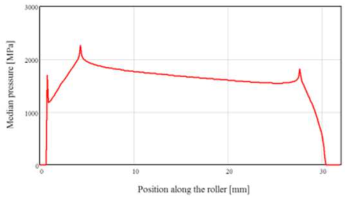	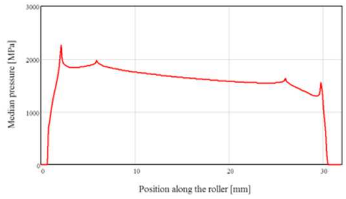
85 kN	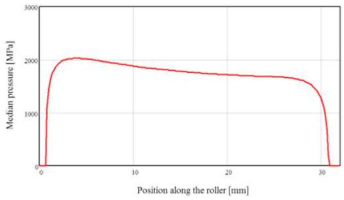	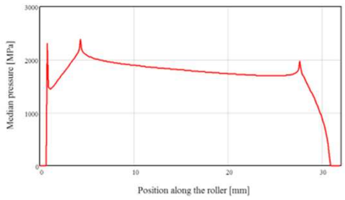	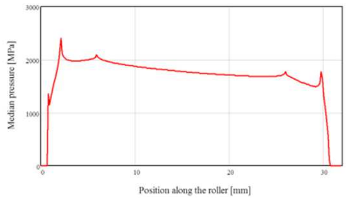
100 kN	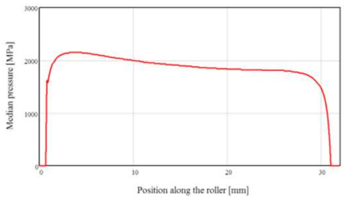	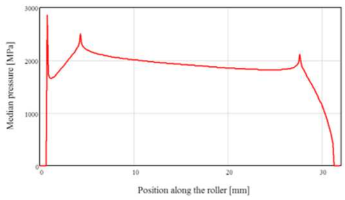	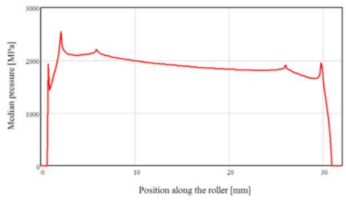
115 kN	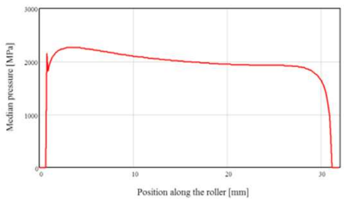	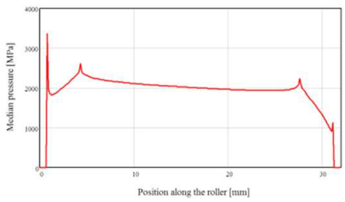	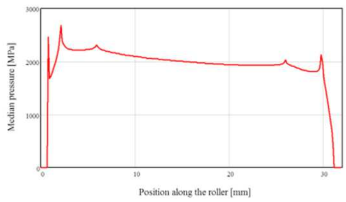
130 kN	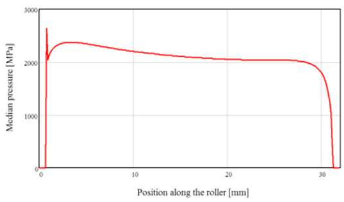	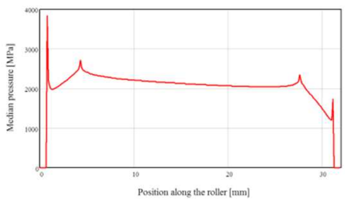	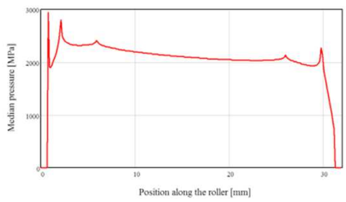
145 kN	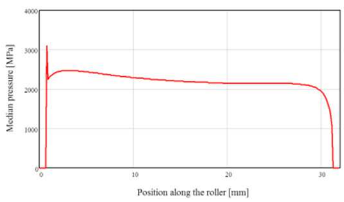	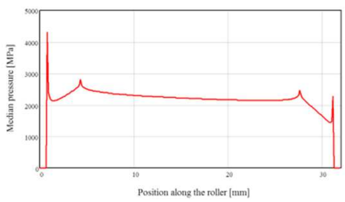	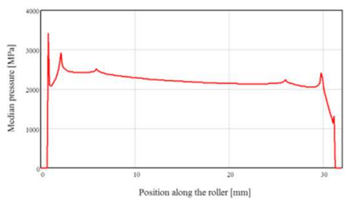

Table A2. Loading case III. Contact pressure distribution (between the roller and IR raceway).

F_r	Optimal profile	Profile A	Optimal approx. profile
70 kN	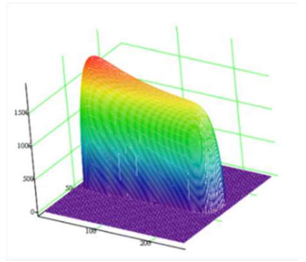	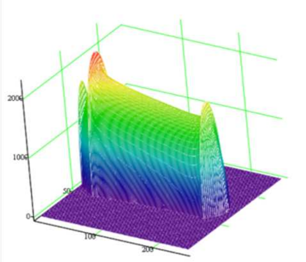	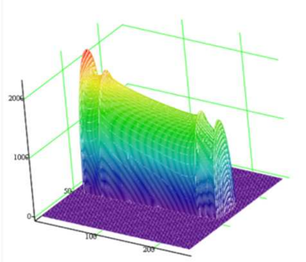
85 kN	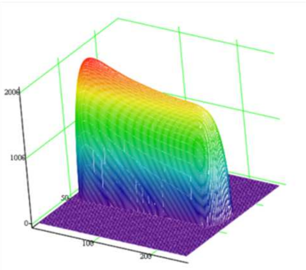	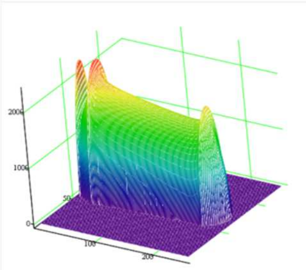	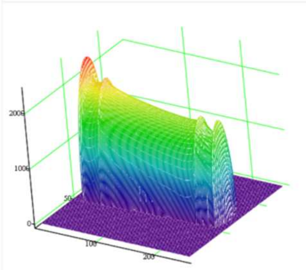
100 kN	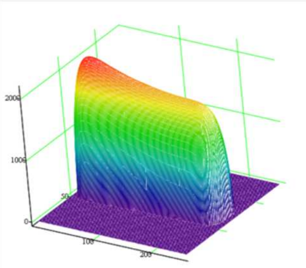	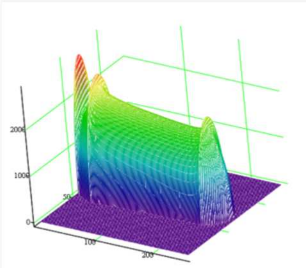	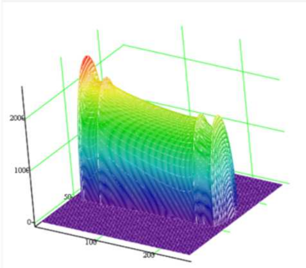
115 kN	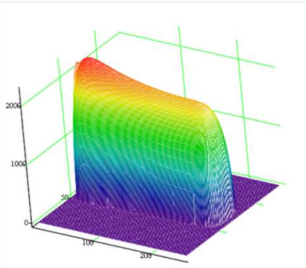	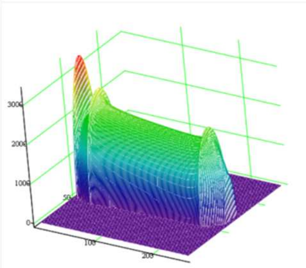	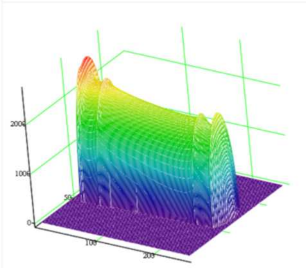
130 kN	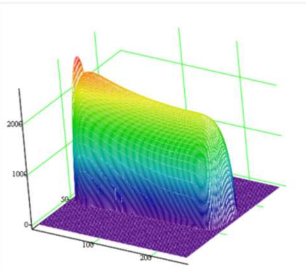	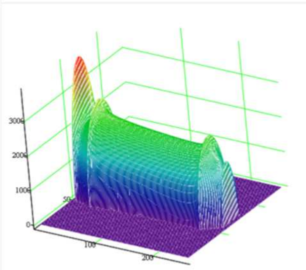	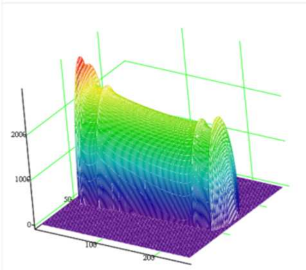
145 kN	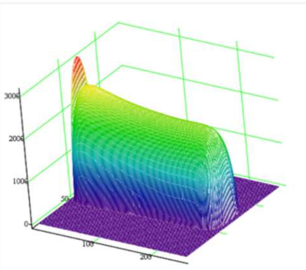	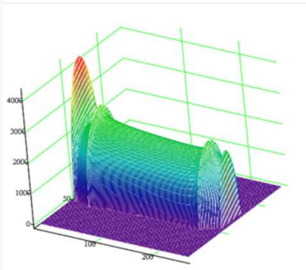	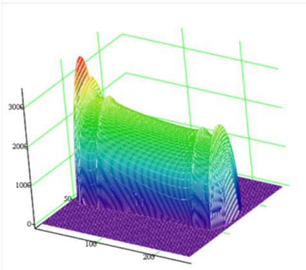

Table A3. Loading case III. Maximum von Mises stress in the inner ring.

F_r	Optimal profile	Profile A	Optimal approx. profile
70 kN	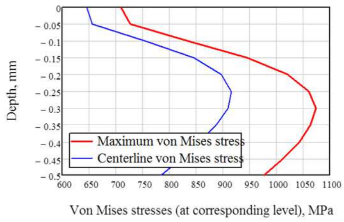	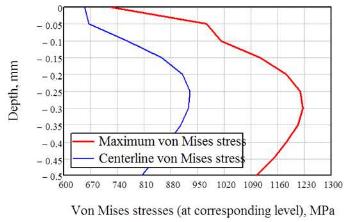	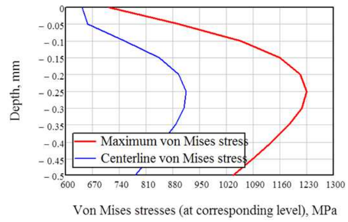
85 kN	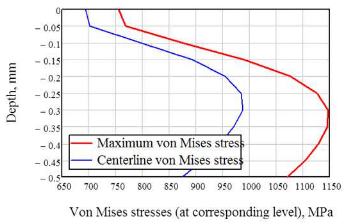	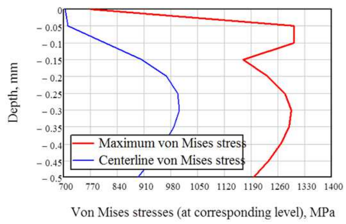	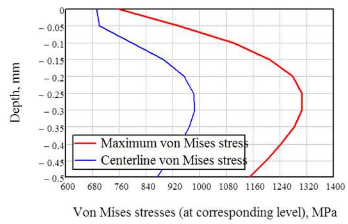
100 kN	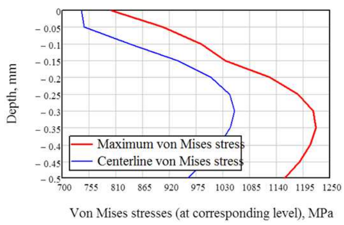	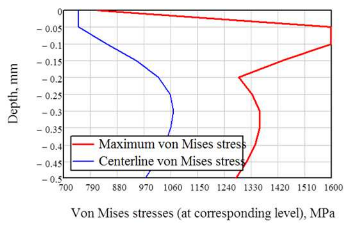	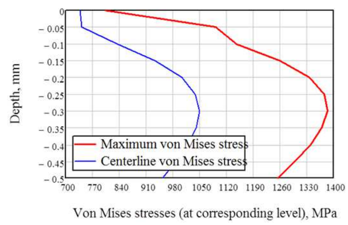
115 kN	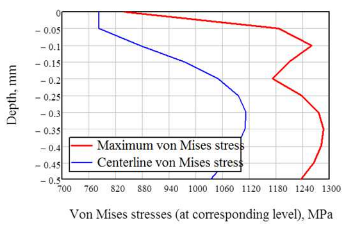	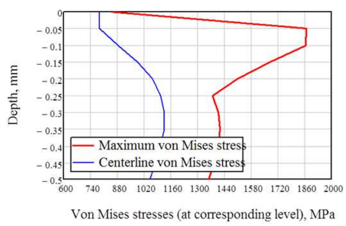	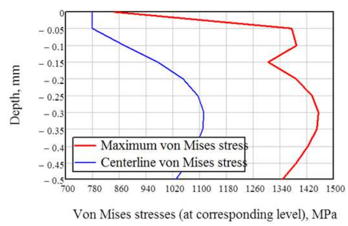
130 kN	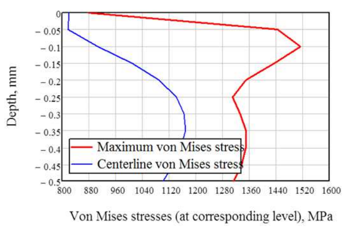	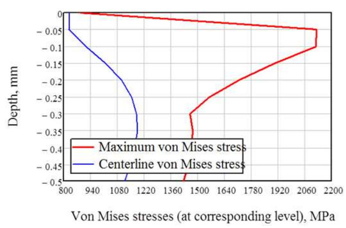	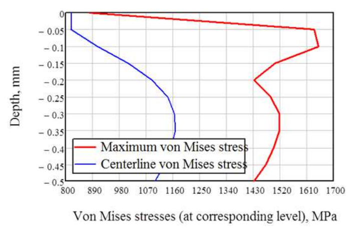
145 kN	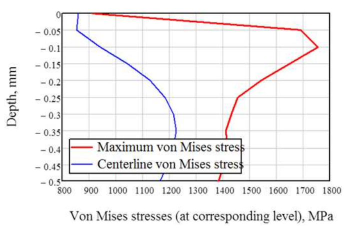	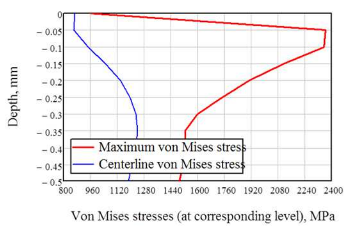	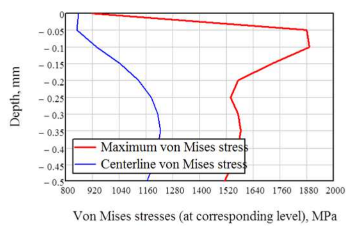

IOP Conf. Series: Materials Science and Engineering **393** (2018) 012002 doi:10.1088/1757-899X/393/1/012002

Table A4. Loading case III. Von Mises stress in the inner ring at the depth it reaches its maximum.

F_r	Optimal profile	Profile A	Optimal approx. profile
70 kN	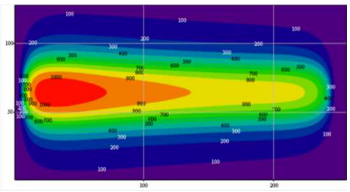	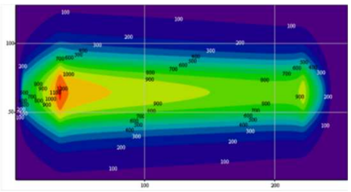	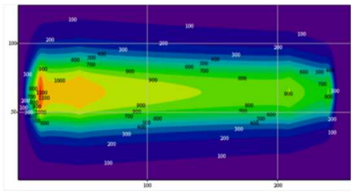
85 kN	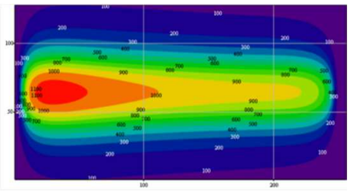	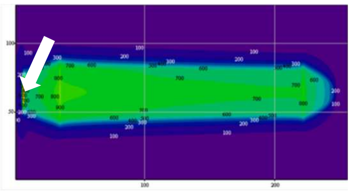	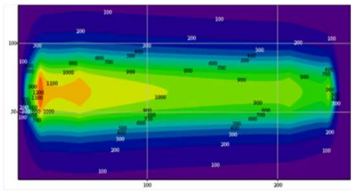
100 kN	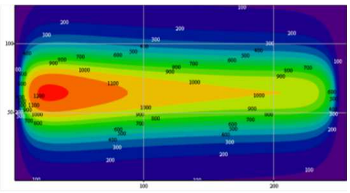	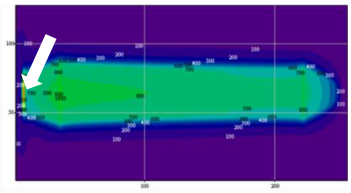	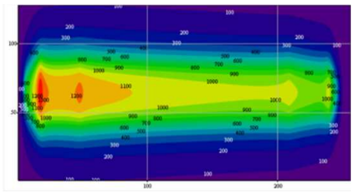
115 kN	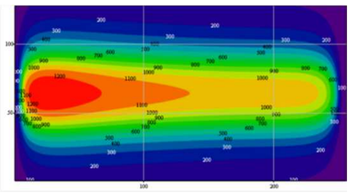	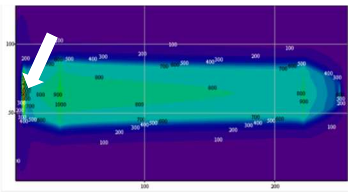	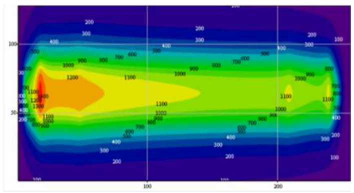
130 kN	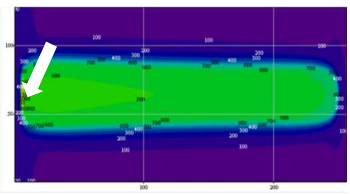	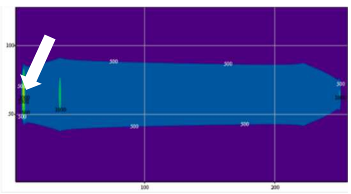	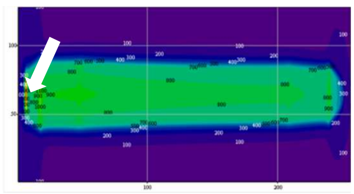
145 kN	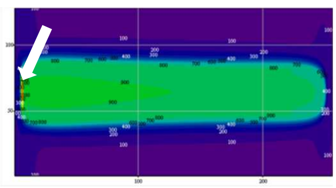	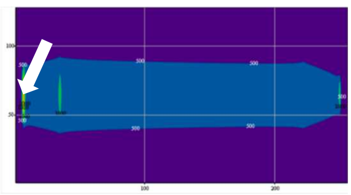	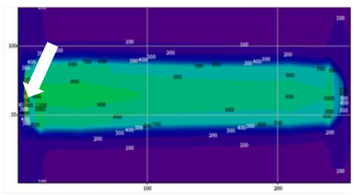

Note: Where needed, white arrows indicate the position of the maximum von Misses stress along the plane parallel to the contact surface.

IOP Conf. Series: Materials Science and Engineering **393** (2018) 012002 doi:10.1088/1757-899X/393/1/012002

References

[1] Harris T A and Kotzalas M N 2007 *Advanced Concepts in Bearing Technology*, CRC Press, Taylor & Francis Group, LLC
[2] Johnson K L 1985 *Contact Mechanics*, Cambridge University Press
[3] De Mull J M, Kalker J J and Fredriksson B 1986 The Contact Between Arbitrarily Curved Bodies of Finite Dimensions, *Journal of Tribology* **108** 40-148
[4] Poplawski J V, Zaretsky E V and Peters S M 2000 *Effect of Roller Profile on Cylindrical Roller Bearing Life Prediction*, Annual Meeting sponsored by the Society of Tribologists and Lubrication Engineers, Nashville, USA, May 7-11, NASA/TM-2000-210368, pp. 1-28
[5] Zhao J 2015 *Fast Solvers for Concentrated Elastic Contact Problems*, Technische Universiteit Delft, The Netherlands, PhD Thesis
[6] Liu S, Wang Q and Liu G 2000 A Versatile Method of Discrete Convolution and FFT (DC-FFT) for Contact Analyses, *Wear* **243** 101-111
[7] Polonsky I and Keer L M 1999 A Numerical Method for Solving Rough Contact Problems Based on the Multi-Level Multi-Summation and Conjugate Gradient Techniques, *Wear* **231** 206-219
[8] Wang Q J and Chung G Y-W (Eds.) 2013 *Encyclopaedia of Tribology*, Springer
[9] Lundberg G 1961 Elastic Contact Between Two Semi-Infinite Bodies, *Fur Schung auf dem Gebieto des Engenienswesens* **10**(5) 165-174
[10] ISO/TS 16281: 2008(E) *Rolling Bearings — Methods for Calculating the Modified Reference Rating Life for Universally Loaded Bearings*
[11] Johns P M and Gohar R 1981 Roller Bearings Under Radial and Eccentric Loads, *Tribology International* **14** 31-136
[12] Lösche T 1987 Capacity Increase Due to Modified Line Contact in Cylindrical and Tapered Roller Bearing, *Ball and Roller Bearings Engineering* **1** 4-9
[13] Fujiwara H, Kobayashi T, Kawase T and Yamauchi K 2010 Optimized Logarithmic Roller Crowning Design of Cylindrical Roller Bearings and Its Experimental Demonstration, *Tribology Transactions* **53**(6) 909-916
[14] Tudose L, Ursache C, Tudose C and Rusu F 2016 *Optimal 2ZB Approximation of Optimal Profile of Rolling Bearings Cylindrical Rollers*, 5th International Conference on Power Transmissions BAPT, Ohrid, Macedonia, October 5-8, pp. 99-113
[15] Hartnett M J 1980 A General Numerical Solution for Elastic Body Contact Problems, *ASME AMD (Am Soc Mech Eng Appl Mech Div)* **39** 51-66
[16] Tudose L, Tudose C and Ursache C 2017 *Optimal Profiles of Cylindrical rollers of Rolling Bearings*, 8th International Scientific Conference on Research and Development of Mechanical Elements and Systems IRMES, Trebinje, Bosnia and Herzegovina, September 7-9, pp. 47-52
[17] Zheng H and Zhou Y 2012 A Novel Cuckoo Search Optimization Algorithm Based on Gauss Distribution, *Journal of Computer Information Systems* **8**(10) 4193-4200
[18] Tudose L, Kulcsar G and Stănescu C 2013 Pareto Approach in Multi-Objective Optimal Design of Single-Row Cylindrical Rolling Bearings, *Power Transmissions, Mechanisms and Machine Science* **13** 519-528
[19] Najjari M 2014 *Characterization of Edge-Contact Influence on Tridimensional EHD Film Shape, Pressure, Stress and Temperature Distribution,* Université de Québec, Canada, PhD Thesis